INTERANNUAL VARIABILITY IN WEDDELL SEA ICE FROM ERS WIND SCATTEROMETER

Mark R. Drinkwater*, Xiang Liu*, Doug Low**, and Peter Wadhams**

*Jet Propulsion Laboratory, California Institute of Technology
4800 Oak Grove Drive, CA 91109, USA
**Scott Polar Research Institute, University of Cambridge
Lensfield Rd, Cambridge, CB2 1ER, UK

ABSTRACT

ERS-1/2 SAR and Wind Scatterometer data are analyzed together with DMSP SSM/I microwave radiometer data to investigate interannual variability in Weddell Sea ice and summer melt signatures during the period 1992-1997. Simultaneous SAR and Scatterometer images were obtained during a February 1995 cruise of the H.M.S. *Endurance* and aerial photographs collected for validation of the satellite observations. Accompanying field data are used to illustrate the observed interannual variability, and to validate the first ever field observations of extensive summer melt ponding in the Weddell Sea, Antarctica. A preliminary algorithm is designed to detect the occurrence of melting in the Weddell Sea, and the date upon which the surface begins to melt. In contrast to melt, conspicuous, anomalous summer increases in sea-ice backscatter reveal a process unique to Antarctic sea ice, involving surface flooding of perennial ice floes and upward meteoric ice growth. Time series data indicate that flooding is particularly widespread, and that subsequent freeze-up in these regions potentially contributes a significant volume of sea ice to the total mass budget of the Weddell Sea.

1. INTRODUCTION

Fundamental differences exist between the Antarctic and Arctic when it comes to spatial and temporal variability in sea-ice conditions in response to seasonal atmospheric and oceanographic forcing. In summer, the Arctic remains largely covered by multiyear ice, surviving each summer melt period by way of its thickness, to accrue incrementally more thickness in winter. Antarctica has no perennial ice counterpart, and for the most part non-landfast sea ice reaches an age of only second-year ice before drifting into high oceanic heat flux regimes and rapidly melting. Sea-ice dynamics regulate the maximum age of the ice cover, particularly in the Weddell and Ross Seas, where the Gyre circulation sweeps sea ice northwards. The relative age and thickness of the residual autumn ice cover is a critical variable to the stability of the upper ocean in these regions, as summer melting helps to freshen and stabilize the mixed layer and together with the residual perennial ice cover prevents complete removal of the summer ice cover.

In the Antarctic, melting largely takes place from beneath the ice, as summer air temperatures rarely rise above 0°C. Consequently, the expression of classical surface melt-ponding has never been observed and the surface retains a snow cover year-round. Conversely, Arctic summer melting results in the expression of melt ponds over up to 60% of the surface as the snow cover disappears completely. Meltwater infiltrates the warm, porous sea ice, flushing out its salt content to leave it relatively brine-free. The fact that the Antarctic snow cover is retained throughout summer helps to insulate the ice and protect it from temporarily warm air temperatures [Ref. 1]. In perennial sea-ice regions, surface flooding can occur with resulting upward meteoric ice growth occurring during autumnal freeze-up [Ref. 2].

In this paper, we study the combined seasonal effects of sea-ice advection and summer melting upon time-varying microwave signatures extracted from a number of fixed regions in the north-western Weddell Sea. The resulting data set extends from 1992-1997, enabling the long-term mean annual signal to be extracted. The residual interannual anomaly time-series illustrates extreme variations in regional melting and/or sea-ice dynamics.

2. DATA SETS

Several active and passive satellite microwave data sets were combined with field data from the north-western Weddell Sea. Synthetic Aperture Radar (SAR) images (100×100 km) and wind scatterometer data were collected by the ERS-1 and 2 spacecraft (hereafter EScat). The latter were processed into images at 3 day intervals [Refs. 3, 4] for the period 1992-97. EScat measured the vv-polarized normalized backscatter coefficient σ°_{vv} (dB) along a 500 km-wide swath and the backscatter at a mid-swath incidence-angle of 40^{o} is expressed as *A*. A number of EScat sample boxes are defined and numbered in the North-western Weddell Sea, in Fig. 1. Additional coincident daily SSM/I data were extracted from these regions and used to confirm melting. Passive microwave brightness temperature (T_b) values approach a blackbody response (*i.e.* close to 273 K) at the melt-point of sea ice.

Pairs of overlapping ERS-1 SAR swath data were acquired on 11 and 14 February (orbits 18704 and 18747), and 12 and 15 February, 1995 and mosaicked. In Fig 1 the descending and ascending strips (dashed) span several hundred kilometer long transects. These crossed the open ocean limit of the marginal ice zone (MIZ) at around 65° S into high concentration (> 95 %) perennial ice south of 67° S.

Coincident field data were acquired between 10-15 February, 1995 from H.M.S. *Endurance* [Ref. 5]. The British Royal Navy icebreaker positioned herself to collect simultaneous *in-situ* data during ERS-1 overpasses. One helicopter facilitated surface data collection while another was equipped for aerial photography. The 11 and 14th February descending pair of SAR swaths were acquired during local daylight (09:25hrs), thereby enabling detailed air-photo comparisons.

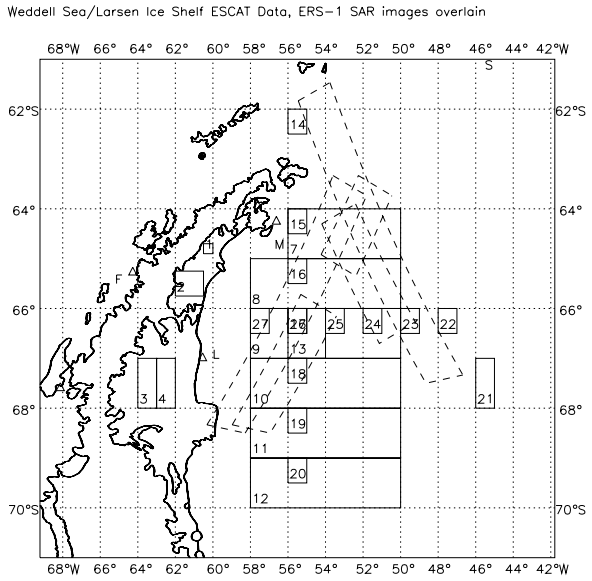

Figure 1. *Weddell Sea map indicating numbered sample boxes for EScat and SSM/I data, overlapping ERS-1 SAR mosaics (dashed) on 11 and 14 February, 1995, and meteorological stations (triangles) situated at Faraday (F), Marambio (M), and the Larsen Ice Shelf (L).*

3. SEASONAL TO INTERANNUAL VARIABILITY

Time series microwave signatures extracted from the sea-ice boxes in Fig. 1 show variability indicative of seasonal and annual changes in the characteristics of the snow and ice floe surfaces together with the proportions of ice types advected through each region. To rule out dynamic effects, four control regions (1-4) were investigated on the Larsen Ice Shelf (LIS) in conjunction with meteorological station data. Results from box 3 are shown in Fig. 2. The upper panel indicates a large dynamic range in *A* values as a result of austral summer melt as far as 68° S. Decreases of -20 dB or more occur during active surface melting, and melting is confirmed by concurrent SSM/I 19 GHz v-polarized T_b values tending to 273 K. The middle panel indicates the 5-year mean annual and filtered cycles, and the lower anomaly cycle is the result of removing the %-year mean from the record. Clearly, the summers of 1992/93 and 1994/95 were anomalous, each with earlier and more extended melt seasons. These years coincide with events marking rapid disintegration of the northern section of the LIS together with the landfast ice between James Ross Island and the peninsula [Ref. 7]. Also the calving of a spectacular iceberg occurred close to box 2 in early 1995 [Ref. 7].

Variability in EScat *A* values is also investigated in two other regions in Fig 3. The advection of varying fractions of seasonal or perennial ice through each box is responsible for the large seasonal amplitude in Fig. 3a and b. Oscillations in *A* during minimum ice extent in box 15 indicate that wind-roughened open water is not responsible for any values exceeding -15 dB in this box. This is typical in stable summer atmospheric boundary layers in the MIZ. Notably, Fig. 3a shows minima in the summer months. April and May peaks in *A* are typical of high perennial ice concentrations, and show a gradual decline until October. 1992 and 1995 ice seasons suggest large fluxes of old ice (> -10 dB) through this box [Ref. 3], marking the disintegration of fast ice along local parts of the peninsula. To corroborate this, swarms of large floes of perennial ice with > 1 m deep snow were observed during WWGS '92 [Ref. 6]. Figure 3a also shows abrupt melt onsets in late 1992 and '95, consisting of sudden drops of 5 to 7 dB.

Fig. 3b shows an extremely different signal in southern box 20. Peak *A* values now occur in austral summer in contrast to box 15 minima. A seasonal decline in *A* values during winter marks diffusion of residual perennial sea ice and advection of an increasing fraction of seasonal sea ice through this region in response to northwards drift of ice away from the Ronne-Filchner ice shelf polynya [Ref. 3].

The distinctive seasonal cycle and maxima in Fig. 3b characterize 1992 surface-flooding signatures documented during Ice Station Weddell (ISW) [Ref. 2]. Snow-covered perennial ice floes surrounding ISW increased their σ°_{vv} values in austral summer as a result of ice-surface flooding beneath the snow. Since air temperatures at this latitude are typically too cold for melting, the snow must insulate the ice sufficiently to become isothermal, by heat supplied from beneath. If the snow cover is deep enough for an isostatic imbalance [Ref. 1] then it may flood with seawater through open brine drainage channels, causing a widespread increase in σ°_{vv} [Ref. 2].

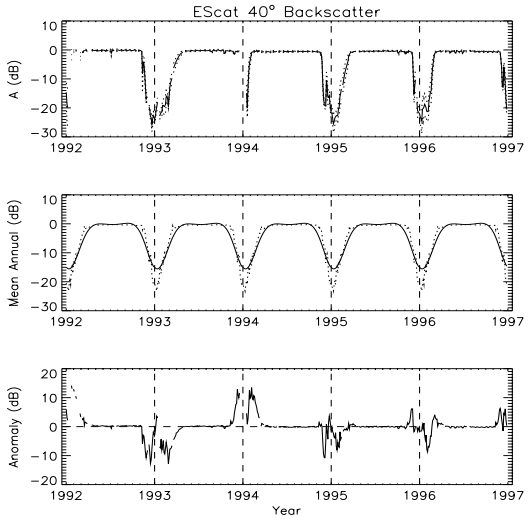

Figure 2. *(a) Interannual; (b) mean seasonal cycle; and (b) anomaly time series from the Larsen Ice Shelf (box 3).*

a.

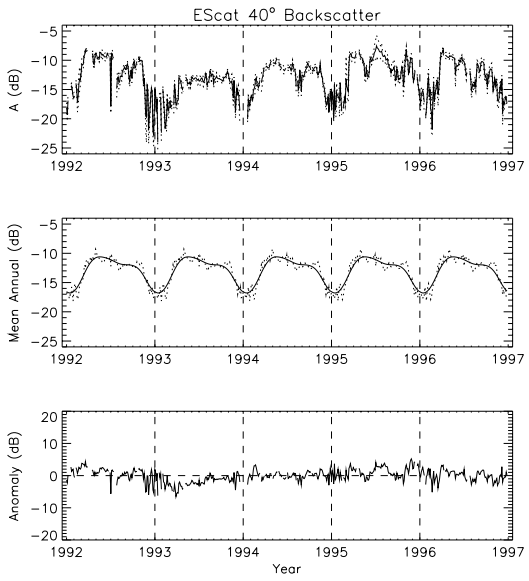

b.

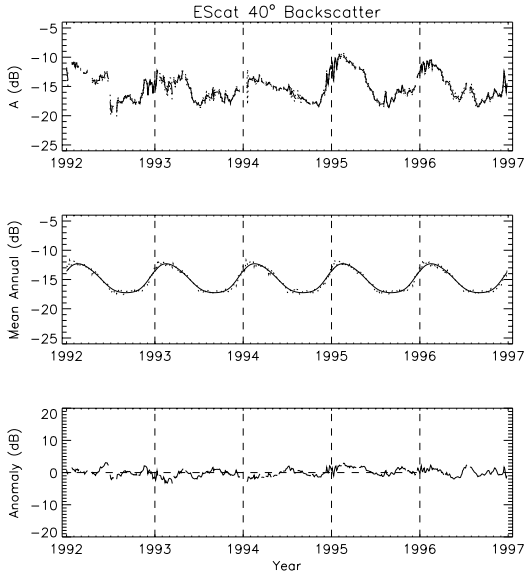

Figure 3. *Interannual time series from (a) box 15; and (b) box 20, in the geographic locations of the H.M.S. Endurance Experiment and Ice Station Weddell, respectively.*

4. SUMMER SCATTERING SIGNATURES

In the southernmost boxes, austral summer results in a signal with opposite sense to boxes experiencing direct surface melting. Dramatic reductions in the summer backscatter in seasonal ice regions can only be associated with the onset of snow-surface melting, particularly in boxes near to the meteorological station Marambio, where air temperatures are well known. SSM/I observations concur by exhibiting blackbody temperatures during periods of warm air temperatures and surface melting.

4.1 Snow Surface Melt and Melt Ponding

Surface melt is demonstrated to have a significant effect upon regional signatures in the north-western Weddell Sea. *In-situ* observations of melting made in February 1995 explain the widespread reduction in *A* values in box 7, 8, 15, and 16. Fig. 4 shows a 10 km vignette of an ERS-1 SAR scene obtained coincident to aerial photographs made from Endurance (centered on white spots). The photograph from the highlighted box indicates the lower left edge of the large floe, approximately 6 x 7.5 km in size, situated 100 km inside the ice edge at 65.85°S 55.75°W. The anomalous appearance of large melt ponds up to 50m across is evident on the large floe. Similar ponding is also observed on smaller ice floes (15-200m in diameter) seawards to within 2-3 km of the ice edge before floes were too small to support surface ponds. Measurements also indicated that such perennial floes were typically 2.5-4m thick with a 2-15 cm deep snow cover.

Thus, perennial ice in northern Weddell Sea experiences classical melt-ponding during particularly warm summers. Ponds are

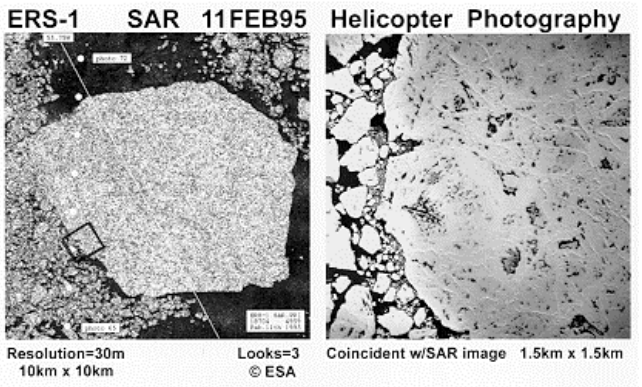

Figure 4. *ERS-1 SAR image (left panel) and coincident aerial photograph (right panel) from black box indicating surface melt ponding.*

expressed in topographic low points on the surfaces of conglomerate ice floes with significant relief. However, the areal extent of melt ponding does not appear to have a significant enough impact at 23° incidence, such that melt ponds are clearly expressed in the high-resolution, filtered 16-bit SAR data. As previously explained in [Ref. 8], this may be due to the fact that rough-surface scattering from high-relief portions of ponded surfaces dominate backscatter signatures.

A preliminary algorithm has been designed to detect the occurrence of melting in the Weddell Sea. A blow up of the 1994-95 melt transition is shown for box 15 in Fig. 5. The melt detection algorithm is presently configured to detect an onset of surface melt characterized by an abrupt decline in backscatter of more than -5

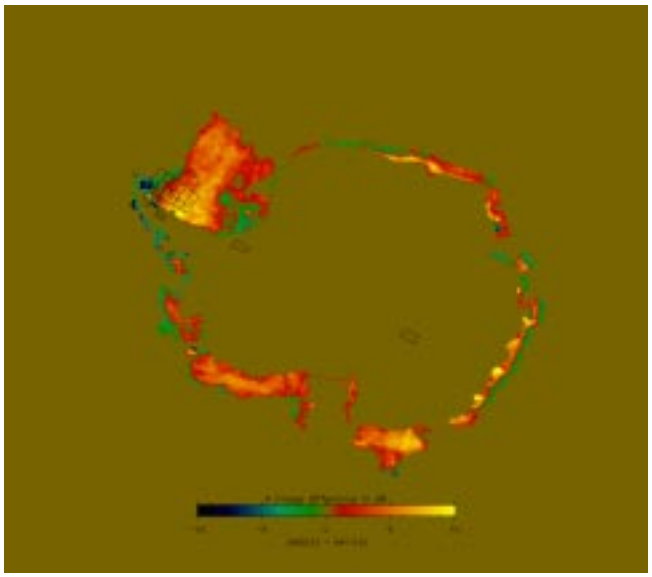

Figure 5. Difference image expressing the pre-summer and mid-summer melt backscatter contrast.

dB, over a contiguous time period exceeding 9 days. The top panel in Fig. 6 indicates a reduction in backscatter of 7 dB over a period of 21 days (or seven images spaced at intervals of 3 days) in the region observed to be melting in 1995. The accompanying plot of

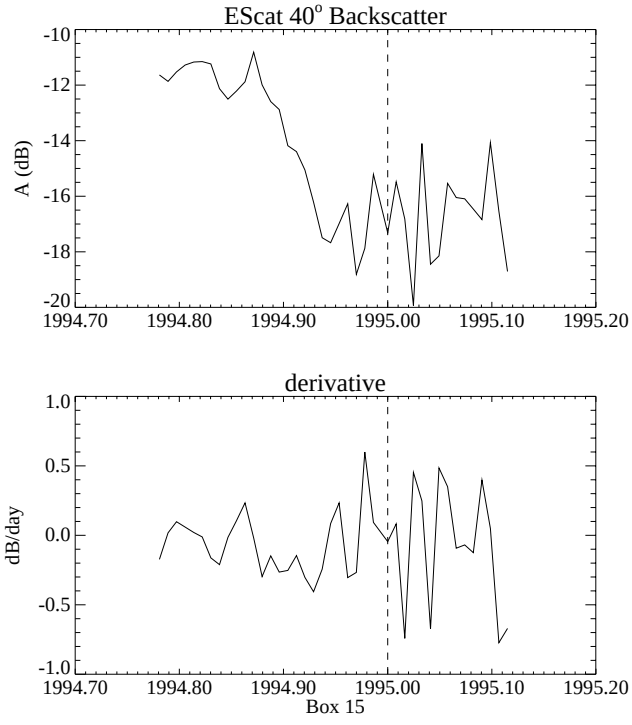

Figure 6. *Box 15 melt transition, expressed as; (a) A values; and (b) its time derivative. The vertical dashed line indicates the end of the 1994 calendar year.*

$\delta A/\delta t$ in the lower panel of Fig. 6 indicates that the time derivative also remains negative for a period of 8 consecutive images, or 24 days. The combination of these two criteria has the advantage of filtering out small rapid fluctuations occurring as a result of mid-winter storms or oscillating spring air temperatures.

To spatially characterize the expression of surface melting, a simple snapshot difference image is generated in Fig. 6 to indicate the backscatter contrast between typical winter, 12 November 1994 (*i.e.* pre-melt), conditions and 12 February, 1995, summer conditions (*i.e.* active melting). Blue and green colors indicate negative differences ranging between -10 and 0 dB, while red or orange tones indicate locations where summer backscatter increased. Negative values indicate the widespread occurrence of melting, particularly around the outer ice margin where air temperatures reach their maximum values in summer.

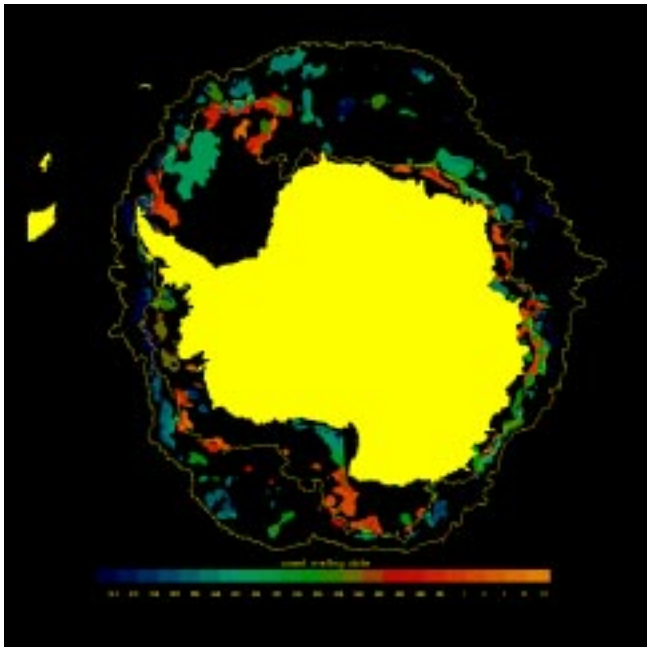

Figure 7. *Estimated dates of Antarctic-wide melt onset, with ice-margin contours spanning the maximum and minimum ice extent during the period shown. The land-masked region is shown in yellow.*

A preliminary example of the final automated melt-detection algorithm result is shown in Fig. 7 for the 1994-95 melt transition. When the onset of melting occurs the algorithm records the date of the onset of melting in the pixel where the threshold, described above, was exceeded. The pre-melt ice margin location and the ice margin corresponding with the end of the melt transition period are shown to indicate the extent of sea-ice margin recession during the early melt season. Colorized regions indicate the date of first occurrence of melting. Surface melting is clearly not widespread nor spatially contiguous at any given instant of time during the

onset of summer. The result indicates that melting occurs in patches, the location of which is likely dominated by the location of storm tracks supplying warm air masses. Perhaps more importantly, results similar to that in Fig. 7 confirm that atmospheric induced surface melting, and resulting albedo feedback is not the dominant sea-ice removal mechanism in summer; but instead, that the oceanic heat flux and short-wave radiation absorbed by the ocean surface in small lead fractions is more effective in removing the summer sea ice cover.

4.2 Flooding

South of the seasonal melt front, the snowcover rarely experiences surface melting, and the snow-ice interface appears to have the more dominant effect on seasonally varying backscatter signatures. As previously explained, high snow loading and basal melting can cause isostatic imbalance, flooding, and upward meteoric ice growth [Ref. 2]. In 1992, at ISW, resulting slushy, saline and high permittivity basal snow enhanced summer σ°_{w} values. Presently, there is no evidence to suggest that flooding does not also occur on perennial ice floes further to the north, but at some point snow surface melting masks any ice surface scattering signal. The effects of surface melting are clearly seen in the south-western Weddell Sea, where summer increases in backscatter often exceed 5 dB. This feature of the Antarctic sea-ice cover is extremely unique and the widespread nature of summertime increase suggest that summer flooding is commonplace. Another location where extremely large summer backscatter contrast is observed is Lutzow-Holm Bay near the Japanese Syowa base (68°S 37°E). Japanese surface measurements [Ref. 9] confirm the localized occurrence of upward meteoric ice growth in association with surface flooding effects in this region.

5. CONCLUSIONS

EScat σ^{o} trends are explained primarily by changes in air temperature and secondly advection of different ice types into/out of the study regions. Results indicate significant interannual variability in the duration and intensity of the melt season, particularly in the north-western region off the east coast of the Antarctic peninsula. The austral summer warming in 1992/93 and 1994/95 was relatively intense, with the anomalous appearance of Antarctic melt ponds, observed for the first time in February 1995. Summer surface melting is expressed in different ways in the microwave data depending on whether north or south of the seasonal isotherm corresponding with snow melting. It would appear from the interannual record that expression of surface melt ponding may more widespread in this region than originally thought, judging from the occurrence of such a melt signature in other years. Similarly the observation of summer increases in backscatter indicates the widespread nature of processes leading to upward meteoric ice growth, more commonly known as snow-ice. Since most thermodynamic models to not adequately represent this process, these results are expected to shed new light on the seasonality and regionality of this unique Antarctic ice-growth process.

Ongoing work involves further development of the capability to use large-scale tracked ice kinematics products from scatterometer and SSM/I images in conjunction with these interannual time series. Dynamical information such as opening/closing will facilitate correction of the time series, such that advective and dynamic influences upon the backscatter variability may be removed. On this basis, smart algorithms may be developed to extract thermodynamically-driven features from the corrected regional melt signatures such as the fraction of ponded or flooded area.

6. ACKNOWLEDGEMENTS

Thanks are expressed to Peter Wadhams for instigating the H.M.S. *Endurance* field measurement campaign and to BAS for supplying meteorological station and AWS data. MRD and XL completed this work at Jet Propulsion Laboratory, California Institute of Technology under contract to the National Aeronautics and Space Administration and funded by Prasad Gogineni of NASA Code YS.

7. REFERENCES

1. Massom, R., M.R. Drinkwater and C. Haas, Winter Snowcover on Sea Ice in the Weddell Sea, *J. Geophys. Res*., 102, C1, 1101-1117, 1997.
2. Drinkwater, M.R., and V.I. Lytle, ERS-1 SAR and field-observed characteristics of austral fall freeze-up in the Weddell Sea, Antarctica, *J. Geophys. Res*., 102, C6, 12593-12608, 1997.
3. Drinkwater M.R., D.G. Long, and D.S. Early, *ESA Journal* 17, 307-322, 1994.
4. Early D.S., and D.G. Long, Resolution Enhancement of Scatterometer Data, *IEEE Trans. Geosci. Rem. Sens*., In Press.
5. Low, D.G., The Validation of ERS-1 SAR Data For Antarctic Summer Sea Ice, Unpublished M.Sc. Thesis, University of Dundee, 143pp., 1995.
6. Drinkwater, M.R., and C. Haas, Snow, Sea-Ice and Radar Observations during ANTX/4: Summary Data Report, *Berichte aus dem Fachbereich Physik*, 53, Alfred Wegener Institut für Polar- und Meeresforschung, Bremerhaven, Germany, 58 pp., 1994.
7. Rott, H., P. Skvarca, and T. Nagler, Rapid Collapse of Northern Larsen Ice Shelf, Antarctica, *Science*, 271, 788-792, 1996.
8. Drinkwater, M.R., and F.D. Carsey, Observations of the late-summer to fall transition with the 14.6 GHz SEASAT scatterometer, *Proc. IGARSS '91*, 3, 1597-1600, 1991.
9. Kawamura, T., K.I. Oshima, T. Takizawa, and S. Ushio, Physical, Structural and Isotopic Characteristics and Growth Processes of Fast Ice in Lützow-Holm Bay, Antarctica, *J. Geophys. Res*., 102, C2, 3345-3355, 1997.